processes

MDPI

Article

Evaluation of Tight Sandstone Mechanical Properties and Fracability: An Experimental Study of Reservoir Sand—Stones from Lufeng Sag, Pearl River Mouth Basin, Northern South China Sea

Chengyong Peng [1], Jun Zhou [1], Jianshu Wu [1], Mao Jiang [1], Hao Zhang [2,*], Biao Yin [2], Shanyong Liu [2] and Yan Zhang [2]

[1] CNOOC Research Institute Co., Ltd., Beijing 100028, China; pengchy@cnooc.com.cn (C.P.); zhoujun23@cnooc.com.cn (J.Z.); wujsh11@cnooc.com.cn (J.W.); jiangmao@cnooc.com.cn (M.J.)
[2] Key Laboratory of Oil and Gas Resources Exploration Technology, Ministry of Education, Yangtze University, Wuhan 430100, China; 17352644983@163.com (B.Y.); liushanyong@yangtzeu.edu.cn (S.L.); yanzhang@yangtzeu.edu.cn (Y.Z.)
* Correspondence: 2021710229@yangtzeu.edu.cn

Abstract: Reservoir rocks of the Pearl River Mouth Basin's Lufeng Sag have low porosity (average porosity 12.6%) and low permeability (average permeability 16.5 mD), requiring hydraulic fracturing to obtain economic production of oil and gas. To contribute to the understanding of these reservoirs, and to promote successful production in the region, we analyzed the mechanical properties of tight sandstone. Moreover, we introduced the shear/tensile strength factor, in combination with the fracture toughness and horizontal stress difference coefficient, as an innovative approach to characterize the ease of forming a complex fracture network after reservoir fracturing. Based on this, we established a fracability evaluation model suitable for offshore low-permeability sandstone reservoirs by an analytic hierarchy process from the perspective of whether the reservoir can form an effective transformation volume and complex fracture network after fracturing. The results indicate that the primary minerals of the target reservoir are quartz and clay minerals, and the natural fractures are not developed. The mechanical properties exhibit a high Young's modulus (ranging from 30.4 to 34.4 GPa) and high compressive strength (with cohesion between 41 and 45 MPa and an angle of internal friction between 31.0 and 33.5°). The relatively low tensile strength and fracture toughness values are conducive to fracture initiation and extension during the fracturing process. Through the fracability evaluation model constructed in this paper, the depth interval at 4155.1–4172.1 m is identified as a high-quality fractured layer. The results of this study not only provide theoretical guidance for target well and formation selection in the Lufeng Sag, but also have important practical implications for increasing oil and gas production from tight sandstone reservoirs.

Keywords: low-permeability reservoirs; tight sandstone; mechanical properties; fracability evaluation

Citation: Peng, C.; Zhou, J.; Wu, J.; Jiang, M.; Zhang, H.; Yin, B.; Liu, S.; Zhang, Y. Evaluation of Tight Sandstone Mechanical Properties and Fracability: An Experimental Study of Reservoir Sand—Stones from Lufeng Sag, Pearl River Mouth Basin, Northern South China Sea. *Processes* **2023**, *11*, 2135. https://doi.org/10.3390/pr11072135

Academic Editor: Carlos Sierra Fernández

Received: 10 June 2023
Revised: 12 July 2023
Accepted: 14 July 2023
Published: 17 July 2023

1. Introduction

The development of tight reservoirs has positive implications for mitigating energy security issues. The subject of this paper is the Wenchang Formation of the Lufeng 14-4 field. The Lufeng 14-4 oil field is located in the Lufeng Sag in the Pearl River Mouth Basin, approximately 216 km south-east of Hong Kong, with an overall NWW–SEE spreading pattern that is adjacent to the northern fault zone to the north and separated from the Hanjiang Sag by the Haifeng Uplift to the northeast, the Dongsha Uplift to the south, and the Huizhou Sag to the southwest. The stratigraphic amplitude is highly variable, the oil layers are deeper, and the structure is more complex. The Wenchang Formation is a terrestrial deposit with rapid longitudinal and transverse changes in the sand body, and the oil formation is affected by the changes in the sand body and the cutting of faults, resulting

in poor lateral comparability. The Wenchang Formation, as a whole, is interpreted by logs to have a porosity of 10.2% to 14.9% (average porosity 12.6%) and a permeability of 2.4 mD to 52.6 mD (average permeability 16.5 mD), which is generally a low-porosity and extra-low to low-permeability reservoir. The Wenchang Formation, as the main formation for oil and gas exploration in the middle-deep Pearl River Mouth Basin, is rich in oil and gas resources. However, the lack of systematic studies on the impact of the various sub-depressional formations, depositional environments, and diagenetic environments on the reservoirs has restricted the exploration process (e.g., Qingming, 2021) [1].

Understanding reservoir properties (including evaluation of the fracability) and understanding the formation and geological evolution of hydrocarbon reservoirs is critical not only for successful oil and gas exploration and production, but is also central to basin-scale petroleum systems analysis and successful scientific understanding and characterization of a region's active petroleum systems (e.g., Magoon & Dow, 1994; Burton et al., 2019; Schulz et al., 2021) [2–4].

Understanding basin-scale petroleum systems is critical in evaluating the prospects of conventional and unconventional reservoirs and can substantially contribute to exploration success (e.g., Bradshaw, 1993; Weimer et al., 1998; Mello et al., 2021) [5–7]. A petroleum systems approach encompasses both assessment of the present day reservoir properties (as explored in our work here), as well as understanding of the sedimentary basin evolution, ranging from deep-water deposition of sand during varying tectonic and climate states (e.g., Bjørlykke, 2014; Burton et al., 2023; Marghani et al., 2023) [8–10], organic matter deposition and subsequent microbial and thermal degradation (e.g., Peters & Cassa, 1994; Hackley & Cardott, 2016) [11,12], the influence of tectonism (including salt tectonism) on reservoir properties (e.g., Hollis, 2011; Soliva et al., 2016; Burton & Dafov, 2023) [13–15], and the general thermal history, fluid movement, and history of subsidence, erosion, and uplift of a prospective hydrocarbon basin (e.g., Hantschel & Kauerauf, 2009; Allen & Allen, 2013) [16,17]. Overall, much remains to be understood about the development, evolution, and properties of tight sandstone reservoirs (e.g., Shanley et al., 2004) [18].

Fracability evaluation is an important reference basis and key indicator for whether the reservoir can be effectively fractured to obtain economic production of oil and gas [19,20]. Most of the current fracability evaluations are based on shale reservoirs, while few studies have been conducted on tight sandstone reservoirs. Enderlin et al. (2011) argued that material brittleness and toughness determine rock fracability and used Young's modulus and Poisson's ratio to simply characterize the fracability [21]. Chong (2010) introduced the brittleness index (BI) to characterize fracability and argued that fracability is strong where the BI is large [22]. However, the subsequent field practice showed that the places with a large brittleness index did not correspond to high-quality fractured layers one-by-one; to overcome the limitation of single factor, De et al. (2022) took fracture toughness into consideration in the fracability evaluation of sandstone [23]. Enderlin et al. (2011) considered factors such as ground stress anisotropy, natural fracture orientation, combined with logging data, compressive strength, and other mechanical parameter to discuss a comprehensive fracability evaluation index [21]. Fang et al. (2023) used hierarchical analysis to specify the influencing factors of fracturing, with shale brittleness and quartz content as reservoir factors, and natural fractures and diagenesis as geological factors [24]. Mullen et al. (2012) calculated the fracability index of shale by considering the sedimentary stratigraphy, stratigraphic properties, mineral distribution, weak surface orientation, and ground stress field [25]. Junliang et al. (2013) established a fracability evaluation method by using three rock mechanical parameters, Young's modulus, Poisson's ratio, and uniaxial tensile strength [26]. Li et al. (2022) and Bai et al. (2021) established a fracability evaluation method for shale gas using three aspects, including shale brittleness, fracture toughness, and natural weak surface, and divided it into three levels of fracability [27,28].

In light of the unknown reservoir properties of the Wenchang Formation in the Lufeng Sag and the absence of a systematic fracability evaluation model, this paper conducts experiments on microstructural characterization and mechanical testing. It is sug-

gested that the fracability of tight sandstone reservoirs should take into account the size of the reservoir transformation volume and the difficulty in forming complex fracture networks. The brittleness index, tensile/shear strength factor, fracture toughness, and horizontal stress difference coefficient are proposed as fracability evaluation indexes of tight sandstone. It provides a theoretical approach as to whether the target reservoir can be effectively fractured.

2. Materials and Methods

2.1. Sample Preparation

Samples were collected from the Wenchang Formation in the Lufeng Sag at a depth of 4155.1–4172.1 m.

2.2. XRD Analysis

After grinding the rock sample to a particle size of less than 1 mm, the clay is separated by centrifugation and the oriented flakes are prepared. XRD measurements were performed on a MinFlexΠ polycrystalline X-ray diffractometer. A basic framework diagram of this assembly can be seen in Figure 1, which included an X-ray generator with a power of 3 KW, a ceramic X-ray tube with a power of 1.2 KW, and a Cu target vertical goniometer Q/2Q with a goniometric accuracy of 0.0001 degrees.

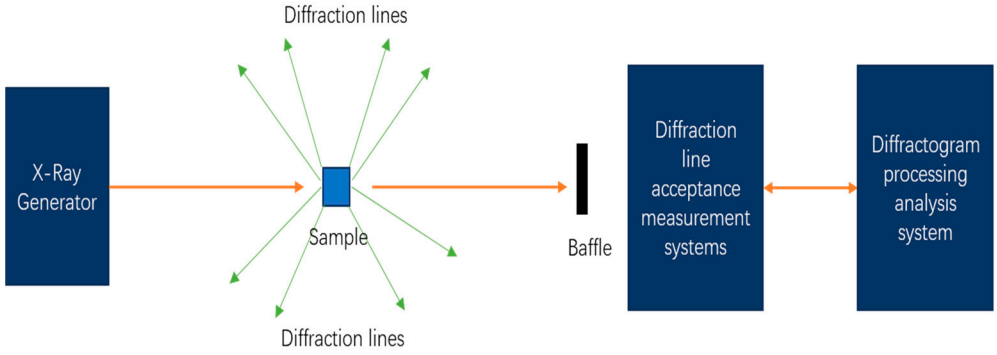

Figure 1. Basic framework diagram of the equipment.

2.3. SEM

The specimens were mounted in the device and evacuated. The samples were imaged using a TM3030 benchtop electron microscope operating at 5 kev and 15 kev. At an accelerating voltage of 5 kev, the amplification is 100×, 200×, and 1000×. At an accelerating voltage of 15 kev, the amplification is 3000×.

2.4. Triaxial Compression Experiment

The cores need to be standardized to the International Society of Rock Mechanics standards prior to the experiment, and the size of the processed rock samples is ϕ25 mm × 50 mm. A diagram of the standard rock sample and a portion of the processed rock sample is shown in Figure 2. Triaxial compression tests were then carried out using the rock mechanics device TAW-2000 Deepwater Pore Pressure Servo Experiment System. The strain of the rock samples was measured by LVDT differential transformer type displacement transducers. The load and strain signals during the experiment are automatically collected, stored, and processed by the computer-controlled HP305A data acquisition control system.

2.5. Brazilian Splitting Test

The Brazilian splitting test is currently the most widely used method for testing tensile strength due to the advantages of the relatively simple specimen preparation and test procedure [29–31]. The rock sample is made to meet the standard dimensions for the test (Figure 3a) and is then fitted into the mold and fixed into the experimental set-up

(Figure 3d). The Brazilian splitting experiments were also carried out using the rock mechanics device TAW-2000 Deepwater Pore Pressure Servo Experiment System with a constant displacement loading pattern until the rock sample underwent tensile damage.

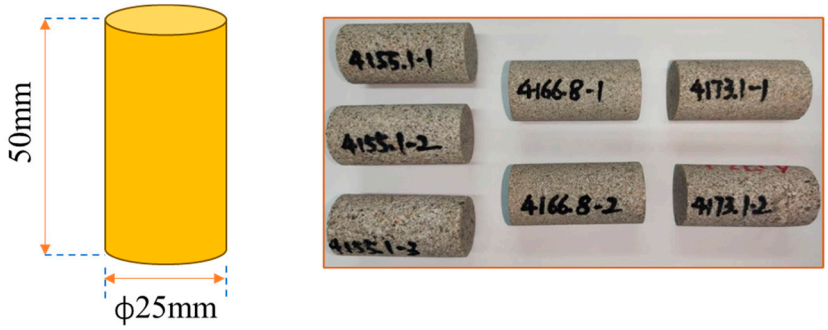

Figure 2. Diagram of the standard rock sample and a portion of the processed rock sample.

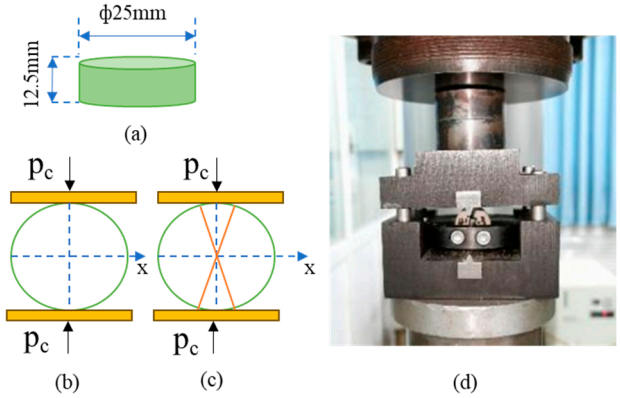

Figure 3. (**a**)The dimensions for the Brazilian splitting test. (**b**) Schematic diagram of the Brazilian splitting test. (**c**) Diagram of rock damage in the Brazilian splitting test. (**d**) Diagram of experimental set-up of the Brazilian splitting test.

2.6. Fracture Toughness Test

Disc-shaped specimens were used to test type I and II fracture toughness [32,33], as in Figure 4. A long straight seam of length 2a (10–12 mm) is prefabricated in the center of the sample to ensure that the ratio of the prefabricated seam to the radius of the sample (a/R) is less than 0.3. Fracture toughness tests were performed on the rock mechanics device TAW-2000 Deepwater Pore Pressure Servo Experiment System. During the experiment, the prefabricated seam is loaded at an angle (0° or 30°) to the direction of loading and a constant displacement loading pattern is used until the rock sample breaks.

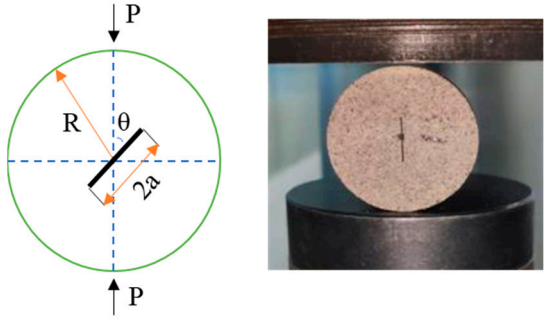

Figure 4. Schematic diagram of the fracture toughness test for disc-shaped specimens.

2.7. Acoustic Emission Experiment

The acoustic emission kaiser effect experiment allows for the determination of the overburden pressure, the maximum horizontal principal stress, and the minimum horizontal minimum principal stress to which the core is subjected in the reservoir state [34–37]. The rock samples required for the experiment need to be cored from different directions, as shown in Figure 5. The experimental system consists of a rock mechanics test system and a PAC acoustic emission test system, as shown in Figure 6. The rock mechanics test system is responsible for applying the load and the acoustic emission test system collects the acoustic emission signals generated inside the core during the loading process.

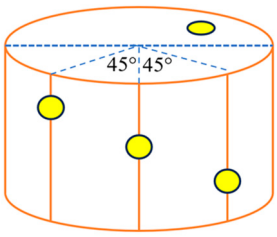

Figure 5. Schematic diagram of coring for the acoustic emission experiment.

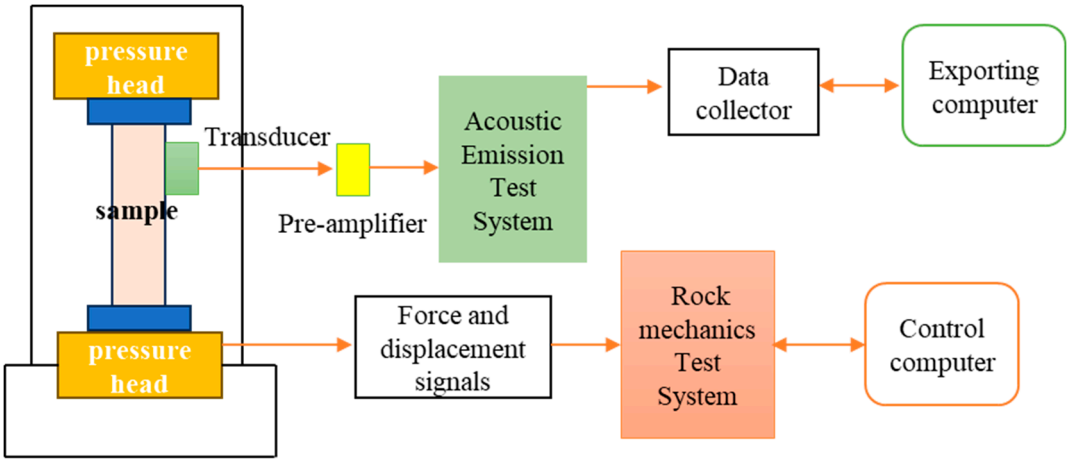

Figure 6. Block diagram of a rock acoustic emission Kaiser effect test system.

3. Fracability Evaluation

Based on the research on the fracability system of tight sandstone and the development practice, fracability is influenced by brittleness index, fracture toughness, natural fractures, ground stress, and other factors [38–41]. The fracability model constructed in this paper integrates the ability to form an effective reformed volume and complex fracture network after fracturing, as shown in Figure 7. Combined with the mechanical characteristics of the region, the brittleness index, shear/tensile strength factor, fracture toughness, and the horizontal difference stress were preferred, taking into account that natural fractures are not developed in Lufeng Sag. Among them, the brittleness index mainly affects the volume of the reservoir reformation, and the shear/tensile strength factor, fracture toughness, and the horizontal difference stress coefficient mainly affect the ease of the complex fracture network formation after fracturing [42].

3.1. Influencing Factors of the Fracability Index (FI)

3.1.1. Brittleness Index

The brittleness index of the rock is the main factor affecting the fracability of the rock and is directly related to the effectiveness of fracturing. The greater the brittleness of the rock, the more microfractures that are induced near the main fracture produced by

hydraulic fracturing, and the more likely they are to form a complex fracture network. There is no clear definition of what brittleness is, and there are different methods of calculation. The two most widely used methods of calculating the brittleness index are based on mineral composition and elastic parameters [43–47].

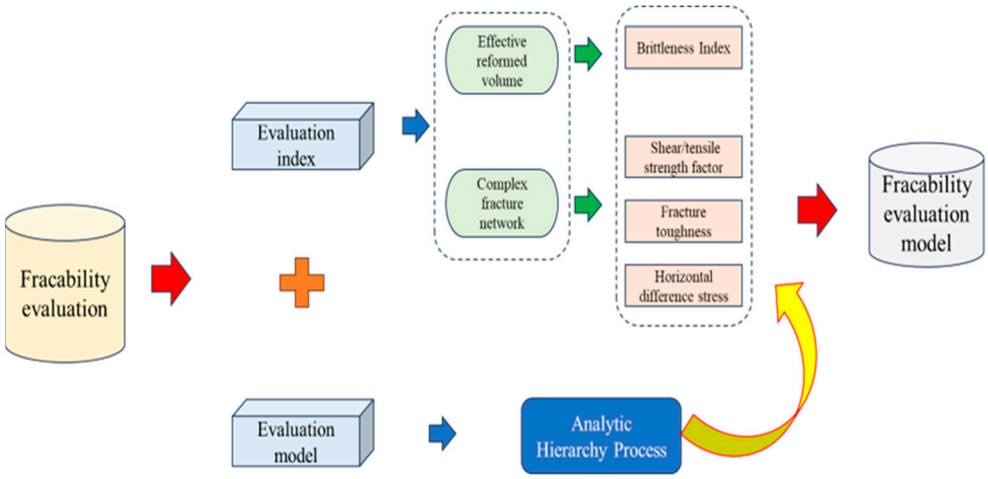

Figure 7. Workflow diagram of fracability evaluation.

The former Is based on the conten" of 'Iittle minerals in the rock and is calculated as in Equation (1) [46]. Brittle minerals mainly include calcite, quartz, and feldspar [46]. The latter is based on the elastic modulus and Poisson's ratio. A high elastic modulus and low Poisson's ratio often imply high brittleness. According to the Rickman brittleness index evaluation method [47], Young's modulus and Poisson's ratio are normalized separately, and the brittleness is described by the mean value of both, as in Equation (4) [47].

$$B_W = \frac{w_{qtz} + w_{feld} + w_{cal}}{w_{tot}} \quad (1)$$

$$E_n = \frac{E - E_{\min}}{E_{\max} - E_{\min}} \quad (2)$$

$$\mu_n = \frac{\mu_{\max} - \mu}{\mu_{\max} - \mu_{\min}} \quad (3)$$

$$B_E = \frac{E_n + \mu_n}{2} \quad (4)$$

To reduce the errors caused by the limitations of the two methods, the rock brittleness is calculated by Equation (5).

$$BI = \frac{B_W + B_E}{2} \quad (5)$$

where BI, B_W, and B_E are the integrated brittleness index, mineral composition-based brittleness index, and elastic parameter-based brittleness index, respectively; w_{qtz}, w_{feld}, w_{cal}, and w_{tot} are the quartz, feldspar, calcite, and total mineral composition masses, respectively; E_n and μ_n are the normalized elastic modulus and Poisson's ratio, respectively; E, $E_{\max}$, and $E_{\min}$ are Young's modulus, the maximum Young's modulus, and the minimum Young's modulus, respectively; μ, $\mu_{\max}$, and $\mu_{\min}$ are Poisson's ratio, the maximum Poisson's ratio, and the minimum Poisson's ratio, respectively.

3.1.2. Shear/Tensile Strength Factor

The ease of creating shear and tension joints during fracturing is important for the formation of complex fracture networks. The rock is prone to tensile damage at a low

confining pressure, while at a high confining pressure, it is mostly shear damage [48]. Shear modulus and tensile strength have a significant effect on the fracturing effectiveness [49]. The greater the shear modulus, the smaller the tensile strength, and the easier the fracture initiation. Accordingly, a shear/tensile strength factor is introduced to characterize the ease of forming complex fracture networks, calculated as in Equation (7). The larger the shear/tensile strength factor, the larger the fracability index.

$$G = \frac{E}{2(1+v)} \tag{6}$$

$$F_{S/T} = \frac{G}{S_t \times 10^3} \tag{7}$$

where G is the shear modulus, GPa; E is the elastic modulus, Gpa; v is Poisson's ratio; $F_{S/T}$ is the shear/tensile strength factor, dimensionless; S_t is the tensile strength, MPa.

3.1.3. Fracture Toughness

Fracture toughness visually reflects the ability of a fracture to extend forward during the fracturing process, which can characterize the ability of fracture extension after fracturing [50]. The smaller the value of the fracture toughness, the less energy required for hydraulic fracture extension and expansion, resulting in more induced fractures and stronger fracability. It is generally accepted that the main types of fractures produced by the fracturing process are type I and type II fractures. Thus, the normalized mean value of fracture toughness measures its fracture toughness, as shown in Equation (8).

$$K_C = \frac{K_{IC-n} + KI_{IIC-n}}{2} \tag{8}$$

where K_C is the fracture toughness index; K_{IC} and K_{IIC} are fracture toughness values of type I and type II, respectively; K_{IC-n} and KI_{IIC-n} are the standardized fracture toughness values.

3.1.4. Horizontal Stress Difference Coefficient

The ground stress affects the direction and morphology of fractured fractures. Generally speaking, the larger the horizontal stress difference, the easier it is to form a single main fracture that extends along the direction of the maximum horizontal principal stress [51]. Considering that the target reservoir is buried deep, the horizontal difference stress coefficient is applicable to represent the influence of horizontal stress difference on FI. The calculation method is shown in Equation (9). A small difference coefficient of horizontal stress is beneficial to reservoir fracturing.

$$K_\sigma = \frac{\sigma_1 - \sigma_3}{\sigma_3} \tag{9}$$

where K_σ is the difference coefficient of horizontal stress; σ_1 and σ_3 are the maximum and minimum horizontal principal stresses, respectively.

3.2. Evaluation Method

In view of the small amount of data on evaluation factors, it is difficult to adopt an objective evaluation method. We have used the Analytic Hierarchy Process (AHP) to qualitatively and quantitatively evaluate reservoir fracability. The AHP can accurately determine the respective weights of influencing factors and the model constructed is a simple linear model [52,53]. Therefore, the fracability evaluation model constructed in this paper can be initially defined as Equation (10).

$$FI = W1 \times BI + W2 \times F_{S/T} + W3 \times K_C + W4 \times K_\sigma \tag{10}$$

3.2.1. Determination of Weights

Modelling by AHP can be broadly divided into 3 steps [54]. The detailed steps are as follows:

Step 1. Establishment of recursive hierarchy

The factors influencing the FI of tight sandstone are clearly defined, and the hierarchical structure is divided into three layers, as shown in Figure 8. The target layer is the characterization of FI for tight sandstone. The criterion layer is the reservoir reformation volume and the ease of formation of complex fracture network after fracturing that affect the FI of tight sandstone. The scheme layer is the specific parameters characterizing the criterion layer, which mainly include the brittleness index affecting the reservoir reformation volume and the parameters changing the ease of forming a complex fracture network after fracturing are the shear/tensile strength factor, fracture toughness, and horizontal stress difference coefficient.

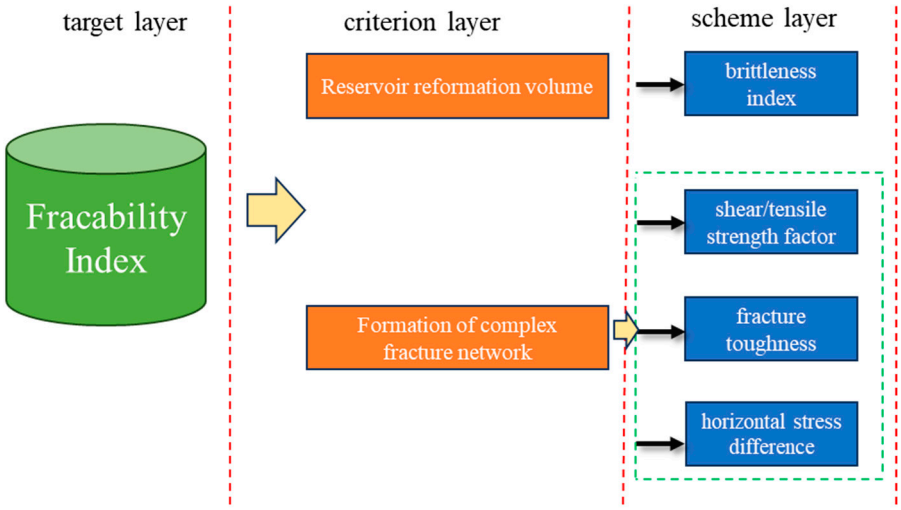

Figure 8. Framework diagram for the Analytic Hierarchy Process.

Step 2. Construction of a comparison matrix

According to the AHP method, a two-by-two comparison judgment matrix is constructed, and the characteristic roots and eigenvectors are calculated. The selected evaluation parameters are compared and assigned values according to their influence on the FI of tight sandstone. For example, A_{ij} indicates the relative importance value of element i (A_i) compared with element j (A_j). The detailed assignment rules are shown in Table 1.

Table 1. Scaling of the comparison matrix.

A_{ij}	Meaning
1	A_i is equally important as compared to A_j
3	A_i is slightly more important than A_j
5	A_i is more important than A_j
7	A_i is more strongly important than A_j
9	A_i is definitely more important than A_j
2, 4, 6, 8,	Median of two adjacent judgments

Step 3. Determination of the weights and consistency of each factor

Weights are calculated by the geometric mean, sum–product, eigenvector, and least squares methods, each of which does not differ significantly. Meanwhile, the consistency

index (CR) is used to test the consistency of the judgment matrix. When the consistency index is less than 0.1, the constructed judgment matrix is considered reasonable.

$$CR = \frac{CI}{RI} \tag{11}$$

$$CI = (\lambda_{\max} - n)/(n-1) \tag{12}$$

$$\lambda_{\max} = \sum_{i=1}^{n} \frac{|Aw_i|}{nw_i} \tag{13}$$

where $\lambda_{\max}$ is the maximum eigenvalue of the comparison matrix, $|A|$ is the value of the comparison matrix A, n is the number of factors, CI is the general consistency index, RI is the average random consistency index, CR is the consistency ratio, and w_i is the weight of the factor in row or column i of the comparison matrix.

3.2.2. Parameter Standardization

Due to the different magnitudes of the brittleness index, shear/tensile strength factor, fracture toughness, and the horizontal difference stress coefficient, the effective range of the values of each parameter will have a large deviation from the FI, and the parameters need to be normalized when substituting into the model calculation [55].

The rock brittleness index and shear/tensile strength factor are proportional to the FI and are positive indicators, which are normalized by Equation (14). The fracture toughness and horizontal stress difference factor are negatively related to the FI and are normalized by Equation (15).

$$S_p = \frac{X - X_{\min}}{X_{\max} - X_{\min}} \tag{14}$$

$$S_n = \frac{X_{\max} - X}{X_{\max} - X_{\min}} \tag{15}$$

where S_p is the standardization of positive indicators, S_n is the standardization of negative indicators, X is the specific assignment of a factor, and $X_{\max}$ and $X_{\min}$ are the maximum and minimum values of the factor.

4. Results and Discussion

4.1. Microstructure of Tight Sandstone

The microstructure of rocks determines the mechanical properties to a certain extent [56], and the development of microscopic fractures also has a significant impact on the effect of reservoir modification. Accordingly, X-ray diffraction (XRD) mineral composition analysis experiments and natural fracture electron microscopy scanning experiments were conducted to study and analyze the microstructural characteristics of tight sandstone.

4.1.1. Mineral Composition

According to the X-ray diffraction experiment results of 24 rock samples, the composition minerals of Wenchang formation in Lufeng Sag are quartz, potassium feldspar, plagioclase, calcite, pyroxenite, square zeolite, barite, and some rock samples contain small amounts of dolomite and rhodochrosite (Figure 9). The XRD patterns of typical samples are shown in Figure 10. The main minerals are quartz and clay minerals with an average percentage of 51.13% and 29.7%, respectively. The high content of brittle minerals (calcite, quartz, and feldspar) has a good foundation for fracability.

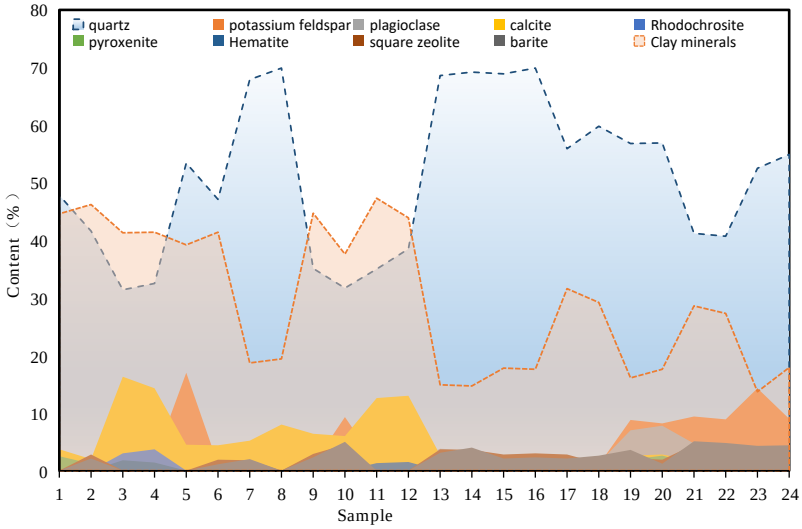

Figure 9. Mineral composition of rock sample (note: each peak in the graph represents the specific mineral content of each rock sample).

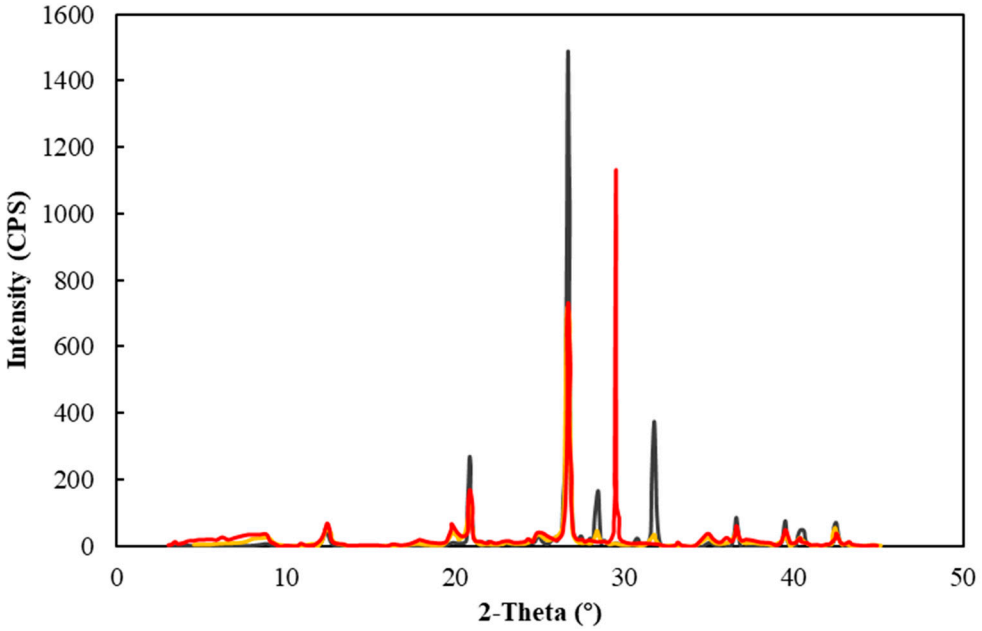

Figure 10. XRD patterns of typical samples.

4.1.2. Natural Fracture

The SEM results showed that the natural fractures in the target reservoir were not developed; only a few intergranular micro-fractures were observed when the magnification reached 1000× or more, and the fracture width was approximately 1 μm to 30 μm (Figure 11). Therefore, the effect of natural fractures can be ignored in the fracability model built for this region.

4.2. Mechanical Properties of Tight Sandstone

Knowledge of regional rock mechanics is an important prerequisite for development planning and the selection of production enhancement methods. The Young's modulus, Poisson's ratio, tensile strength, and fracture toughness all directly affect the formation of the fracture pattern [57,58].

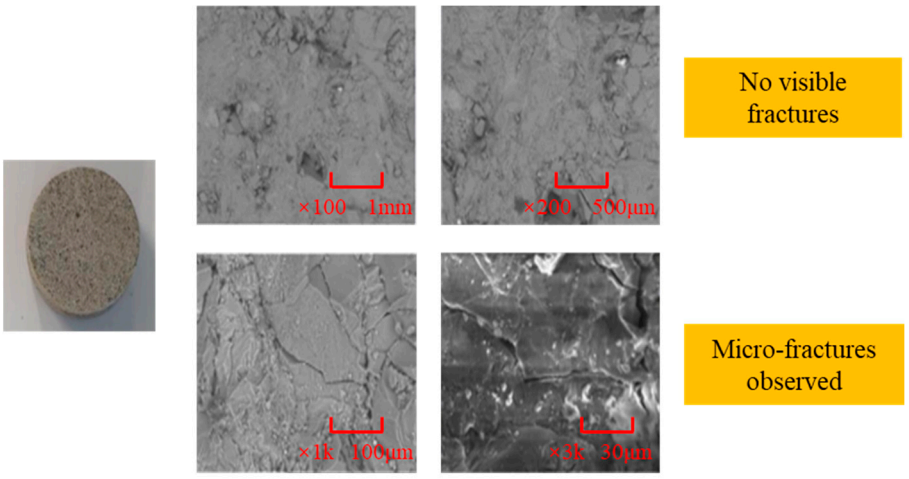

Figure 11. Scanning images by SEM at different magnifications of typical samples.

Triaxial compression tests are used to obtain the elastic parameters (Young's modulus, Poisson's ratio, and shear modulus) and strength parameters (compressive strength, cohesion, and angle of internal friction) of rocks. The experimental results show that the compressive strength and Young's Modulus increase with the increase in the confining pressure. In addition, the test rock samples show typical hard and brittle deformation damage characteristics under different confining pressures, as shown in the stress–strain curve (Figure 12). The data shows a modulus of elasticity of 30.37~30.86 GPa, Poisson's ratio of 0.24~0.28, and compressive strength of 187.99~212.13 MPa at a confining pressure of 20 MPa. The modulus of elasticity is 31.1~31.92 GPa, Poisson's ratio is 0.22~0.28, and compressive strength is 216.35~251.59 MPa at confining pressure of 30 MPa (Table 2). The rocks are mostly shear damaged and the damage characteristics are illustrated in Figure 13. In addition, the shear damage parameters of the target reservoir rocks calculated by combining the experimental results with the Mohr–Cullen shear damage criterion equation are shown in Table 3. The cohesion and friction angle are 41~45 MPa and 31.0~33.5°, respectively, reflecting the high cohesion and denseness of the specimens.

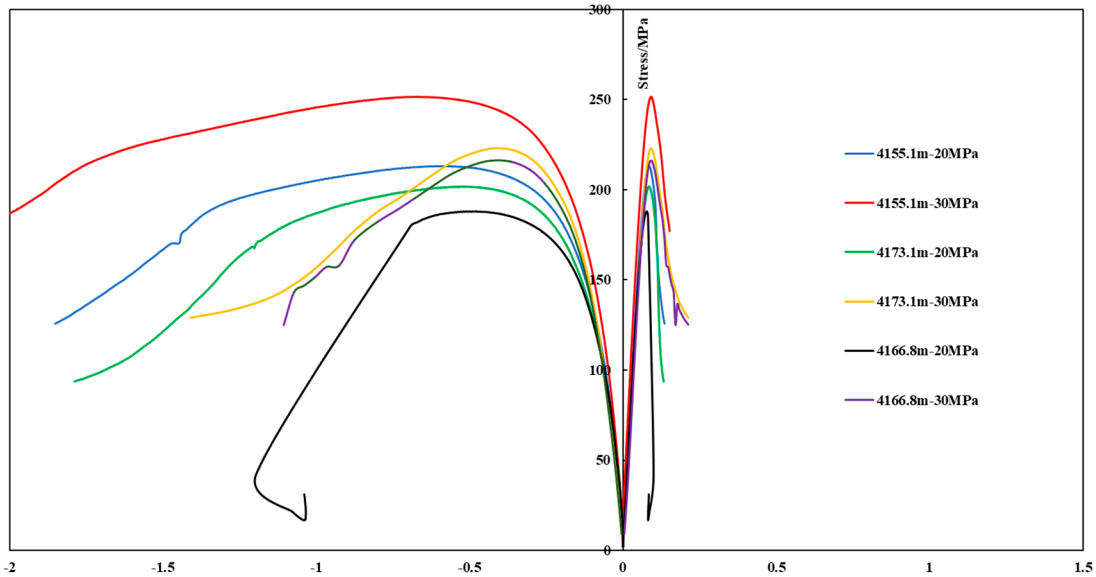

Figure 12. Stress-strain curves of samples.

Table 2. Mechanical parameters of triaxial compression tests.

Well Depth (m)	Confining Pressure (MPa)	Young's Modulus (GPa)	Poisson's Ratio	Compressive Strength (MPa)
4155.1–4172.1	20	30.37	0.28	212.13
		30.86	0.28	187.99
		30.52	0.24	201.86
	30	31.28	0.28	251.59
		31.10	0.26	216.35
		31.92	0.22	222.1

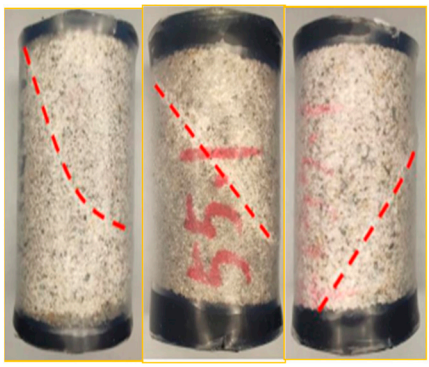

Figure 13. Damage formed on a typical rock sample under triaxial compression conditions.

Table 3. Shear damage parameters of rocks in the target reservoir.

Well Depth (m)	Lithology	Cohesion (MPa)	Angle of Internal Friction (°)
4155.1–4172.1	Tight sandstone	45.31	33.47
	Tight sandstone	41.01	31.10
	Tight sandstone	45.08	31.00

The results of the Brazilian splitting test showed that the tensile strength of the specimens ranged from 3.63 to 4.63 MPa, with a mean value of 4.04 MPa, as shown in Table 4. The overall low tensile strength was prone to tensile damage, which was conducive to the extension of fractures after fracturing.

Table 4. Results of the Brazilian splitting test of rock.

Well Depth (m)	Thickness (mm)	Diameter to Thickness Ratio	Damage Load (N)	Tensile Strength (MPa)
4155.1–4172.1	13.81	0.56	2309	4.34
	13.65	0.56	2433	4.63
	13.47	0.55	1990	3.85
	13.61	0.56	2041	3.91
	12.36	0.55	2309	4.49
	14.03	0.57	1979	3.67
	13.62	0.56	1886	3.63
	12.11	0.54	1886	3.78

The results of the fracture toughness experiment showed that the type I fracture toughness of the reservoir rocks in the target block ranged from 0.263 to 0.304 MPa·m$^{1/2}$ with an average of 0.287 MPa·m$^{1/2}$, and the type II fracture toughness ranged from 0.417 to 0.489 MPa·m$^{1/2}$ with an average of 0.459 MPa·m$^{1/2}$, as shown in Figure 14. The damage pattern of the specimens after the fracture toughness experiments is shown in Figure 15.

The fracture forms are cleavage damage (type I fracture toughness) and shear damage (type II fracture toughness).

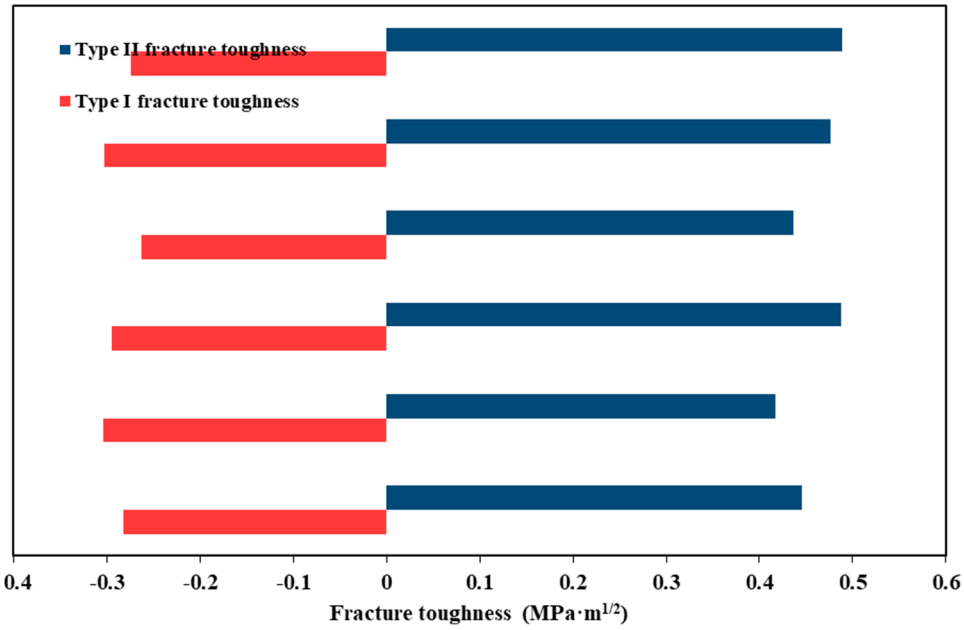

Figure 14. Fracture toughness (type I and type II) of the Wenchang formation.

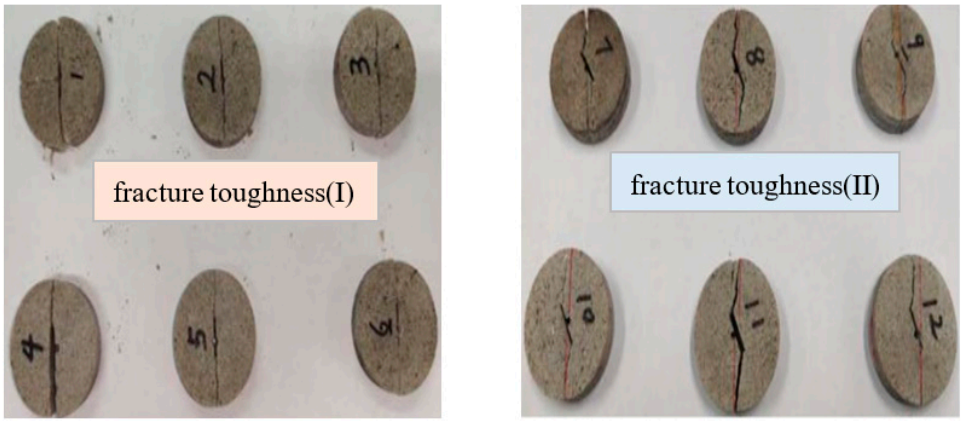

Figure 15. Fracture toughness specimen damage pattern.

Since fracture toughness testing is expensive, many scholars have used statistical methods to establish relationships between fracture toughness and other physical and mechanical parameters [59–61]. Based on the indoor experimental results, the relationship between fracture toughness and tensile strength of the region is fitted, as shown in Figure 16. In conclusion, the fracture toughness of the region is low, which favors fracture initiation and extension.

The acoustic emission experiment results show that the overburden pressure, horizontal in situ stress (max), and horizontal in situ stress (min) equivalent density of 4155.1-4172.1 m tight sandstone in the Wenchang Formation in Lufeng Sag are 1.25 g/cm^3, 1.92 g/cm^3, and 1.57 g/cm^3, respectively, as shown in Figure 17. The stress state of the block belongs to normal faults, and the horizontal stress difference coefficient is less than 0.3, which is conducive to the formation of a complex network of fractures.

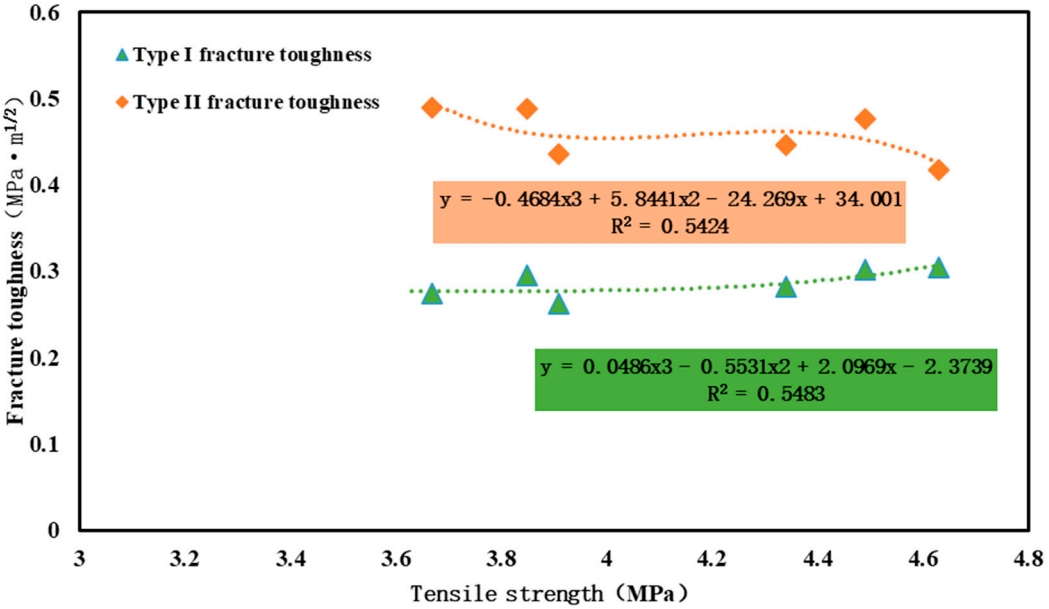

Figure 16. Fitting curve of fracture toughness and tensile strength.

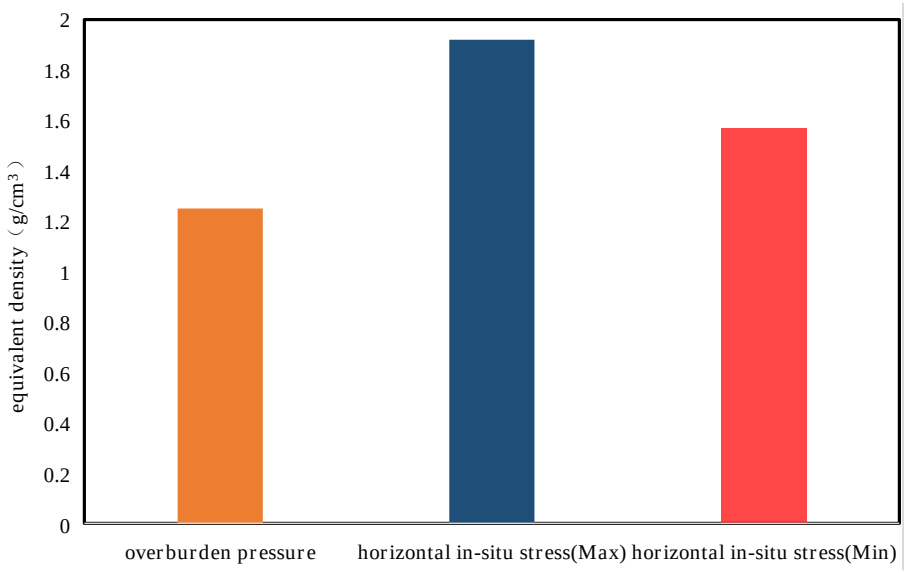

Figure 17. Results of the acoustic emission experiment.

4.3. Evaluation Results

The degree of influence of each parameter with reference to other literature, as well as expert opinions, and the comparison matrix obtained is shown in Table 5.

Table 5. Comparison matrix.

Degree of Importance	Brittleness Index	Shear/Tensile Strength Factor	Fracture Toughness	Horizontal Stress Difference Coefficient
Brittleness index	1	3	2	2
Shear/tensile strength factor	1/3	1	1/2	1/2
Fracture toughness	1/2	2	1	1
Horizontal stress difference coefficient	1/2	2	1	1

Based on the comparison matrix above, the sum–product method was used to obtain the weights, and the calculation results are shown in Table 6.

Table 6. Weighting coefficients of the comparison matrix.

W1	W2	W3	W4	CI	CR
0.42	0.12	0.23	0.23	0.0035	0.0039

According to the results of the analysis, the CR was 0.0138 < 0.1, which satisfied the consistency test. The weights of the brittleness index, shear/tensile strength factor, fracture toughness, and horizontal stress coefficient of variation were obtained as 0.42, 0.12, 0.23, and 0.23, respectively. The fracability index can therefore be calculated by Equation (16).

$$FI = 0.42BI + 0.12 \times F_{S/T} + 0.23 \times K_C + 0.23 \times K_\sigma \quad (16)$$

Combined with the laboratory experiment and relevant reports, the brittleness index, shear/tensile strength factor, fracture toughness, and the horizontal difference stress coefficient of the Wenchang formation rocks in Lufeng Sag were calculated by applying the quantification methods of the factors affecting FI in the above sections. The parameters were substituted into the proposed model, and the calculation results are shown in Figure 18.

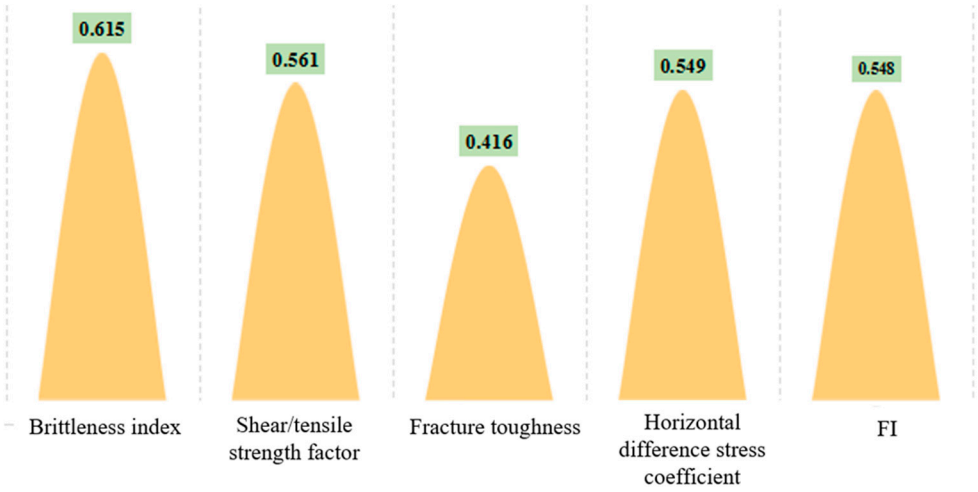

Figure 18. Results of the fracability index of the Wenchang formation.

Drawing on the grading standard of the fracability degree for rock by Yin [62], a comprehensive evaluation standard suitable for offshore low-permeability sandstone reservoirs was established. It is considered that when the comprehensive FI is < 0.3, the fracability of the tight sandstone reservoir is poor; when the comprehensive FI is between 0.3 and 0.5, the fracability is acceptable; when the comprehensive FI > 0.5, the fracability is good. Hence, it can be inferred that 4155.1–4172.1 m of the Wenchang formation in Lufeng Sag is a high-quality fractured layer with a good fracturing effect. This is supported by the fact that the Wenchang formation of well A5 is due to come on stream in April 2022, with a seven-fold increase in daily oil production after fracturing.

5. Conclusions

(1) The Wenchang formation in Lufeng Sag exhibits a mineral composition characterized by "high quartz, high clay," resulting in a high content of brittle minerals and a high brittleness index. This geological characteristic favors the fracturing process, facilitating the economic production of oil and gas.

(2) The rock mechanics of the Wenchang formation in Lufeng Sag are characterized by a "high Young's modulus, high compressive strength, high cohesion, and internal

friction angle." These attributes reflect the rock's denseness. Additionally, the reservoir exhibits low tensile strength and low fracture toughness, indicating its potential to develop a complex fracture network after hydraulic fracturing.

(3) An Analytic Hierarchy Process-based fracability evaluation model is developed for offshore low-permeability sandstone reservoirs, considering the formation's ability to form an effective transformation volume and complex fracture network post-fracturing. This model incorporates factors such as shear/tensile strength, fracture toughness, and the horizontal stress difference coefficient.

(4) The fracability index of the reservoir is calculated as 0.548 using the proposed evaluation model. Specifically, the interval from 4155.1 m to 4172.1 m is identified as a high-quality fractured formation. The findings of this study not only provide theoretical guidance for well and formation selection in the Lufeng Sag, but also have practical implications for enhancing oil and gas production from tight sandstone reservoirs.

Author Contributions: Conceptualization, C.P. and J.Z.; methodology, H.Z.; validation, J.W., M.J. and S.L.; formal analysis, Y.Z., B.Y. and H.Z.; investigation, H.Z.; resources, C.P. and J.Z.; data curation, J.W., M.J. and Y.Z.; writing—original draft preparation, H.Z.; writing—review and editing, B.Y.; visualization, H.Z.; supervision, H.Z. and Y.Z.; project administration, C.P., J.Z., J.W. and M.J.; funding acquisition, S.L. and Y.Z. All authors have read and agreed to the published version of the manuscript.

Funding: The APC was funded by China National Offshore Oil Corporation (CNOOC) 14th Five-Year Plan Major Science and Technology Project: Research on Integrated Geological Engineering Technology for Fracturing and Development of Offshore Low-Permeability Reservoirs (Grant NO. KJGG2022-0701).

Institutional Review Board Statement: Not applicable.

Informed Consent Statement: Not applicable.

Data Availability Statement: The data presented in this study are available on request from the corresponding author.

Acknowledgments: Thank you for the information provided by CNOOC.

Conflicts of Interest: The authors declare no conflict of interest.

References

1. Qingming, C. *Formation Mechanism of Middle-Deep Sandstone Reservoir of Eocene in Zhu I Depression, Pearl River Mouth Basin*; Chengdu University of Technology: Chengdu, China, 2021. [CrossRef]
2. Magoon, L.B.; Dow, W.G. The petroleum system. In *The Petroleum System—From Source to Trap*; Geologists Memoir 60; Magoon, L.B., Dow, W.G., Eds.; American Association of Petroleum: Tulsa, OK, USA, 1994; pp. 3–24.
3. Burton, Z.F.M.; Moldowan, J.M.; Magoon, L.B.; Sykes, R.; Graham, S.A. Interpretation of source rock depositional environment and age from seep oil, east coast of New Zealand. *Int. J. Earth Sci.* **2019**, *108*, 1079–1091. [CrossRef]
4. Schulz, H.M.; Yang, S.; Schovsbo, N.H.; Rybacki, E.; Ghanizadeh, A.; Bernard, S.; Mahlstedt, N.; Krüger, M.; Amann-Hildebrandt, A.; Krooss, B.M.; et al. The Furongian to Lower Ordovician Alum Shale Formation in conventional and unconventional petroleum systems in the Baltic Basin—A review. *Earth-Sci. Rev.* **2021**, *218*, 103674. [CrossRef]
5. Bradshaw, M. Australian petroleum systems. *Pet. Explor. Soc. Aust. J.* **1993**, *21*, 43–53.
6. Weimer, P.; Rowan, M.G.; McBride, B.C.; Kligfield, R. Evaluating the petroleum systems of the northern deep Gulf of Mexico through integrated basin analysis: An overview. *AAPG Bull.* **1998**, *82*, 865–877.
7. Mello, M.R.; Peres, W.; Rostirolla, S.P.; Pedrosa, O.A., Jr.; Piquet, A.; Becker, S.; Yilmaz, P.O. The Santos Basin Pre-Salt Super Giant Petroleum System: An Incredible Journey from Failure to Success. In *The Supergiant Lower Cretaceous Pre-Salt Petroleum Systems of the Santos Basin*; Memoir 124; AAPG: Rio de Janeiro, Brazil, 2021; pp. 1–34. [CrossRef]
8. Bjørlykke, K. Relationships between depositional environments, burial history and rock properties. Some principal aspects of diagenetic process in sedimentary basins. *Sediment. Geol.* **2014**, *301*, 1–14. [CrossRef]
9. Burton, Z.F.M.; McHargue, T.; Kremer, C.H.; Bloch, R.B.; Gooley, J.T.; Jaikla, C.; Harrington, J.; Graham, S.E. Peak Cenozoic warmth enabled deep-sea sand deposition. *Sci. Rep.* **2023**, *13*, 1276. [CrossRef]
10. Marghani, M.M.; Zairi, M.; Radwan, A.E. Facies analysis, diagenesis, and petrophysical controls on the reservoir quality of the low porosity fluvial sandstone of the Nubian formation, east Sirt Basin, Libya: Insights into the role of fractures in fluid migration, fluid flow, and enhancing the permeability of low porous reservoirs. *Mar. Pet. Geol.* **2023**, *147*, 105986.

11. Peters, K.E.; Cassa, M.R. Applied source rock geochemistry. In *The Petroleum System—From Source to Trap*; Memoir 60; Magoon, L.B., Dow, W.G., Eds.; American Association of Petroleum Geologists: Tulsa, OK, USA, 1994; pp. 93–120.
12. Hackley, P.C.; Cardott, B.J. Application of organic petrography in North American shale petroleum systems: A review. *Int. J. Coal Geol.* **2016**, *163*, 8–51. [CrossRef]
13. Hollis, C. Diagenetic controls on reservoir properties of carbonate successions within the Albian–Turonian of the Arabian Plate. *Pet. Geosci.* **2011**, *17*, 223–241. [CrossRef]
14. Soliva, R.; Ballas, G.; Fossen, H.; Philit, S. Tectonic regime controls clustering of deformation bands in porous sandstone. *Geology* **2016**, *44*, 423–426. [CrossRef]
15. Burton, Z.; Dafov, L.N. Salt Diapir-Driven Recycling of Gas Hydrate. *Geochem. Geophys. Geosyst.* **2023**, *24*, e2022GC010704. [CrossRef]
16. Hantschel, T.; Kauerauf, A.I. *Fundamentals of Basin and Petroleum Systems Modeling*; Springer Science & Business Media: Berlin/Heidelberg, Germany, 2009.
17. Allen, P.A.; Allen, J.R. *Basin Analysis: Principles and Application to Petroleum Play Assessment*; John Wiley & Sons: Hoboken, NJ, USA, 2013.
18. Shanley, K.W.; Cluff, R.M.; Robinson, J.W. Factors controlling prolific gas production from low-permeability sandstone reservoirs: Implications for resource assessment, prospect development, and risk analysis. *AAPG Bull.* **2004**, *88*, 1083–1121. [CrossRef]
19. Lihong, Z.; Xuewei, L.; Daqi, F.U.; Dongping, L.; Xingsong, L.; Shengchuan, Z.; Gongquan, C.; Min, Z.; Fuchun, T.; Yudong, Z.; et al. Evaluation and application of influencing factors on the fracturability of continental shale oil reservoir: A case study of Kong 2 Member in Cangdong Sag. *China Pet. Explor.* **2019**, *24*, 670.
20. Jin, X.; Shah, S.N.; Roegiers, J.C.; Zhang, B. Fracability evaluationin shale reservoirs:an integrated petrophysics and geomechanics approach. In Proceedings of the SPE Hydraulic Fracturing Technology Conference, The Woodlands, TX, USA, 4–6 February 2014; p. 168589.
21. Enderlin, M.B.; Alsleben, H.; Beye, R.J.A. Predicting fracability in shale reservoirs. In Proceedings of the AAPG Annual Convention and Exhibition, Houston, TX, USA, 10–13 April 2011; pp. 10–13.
22. Chong, K.K.; Griese, R.W.V.; Passman, A. A completions guidebook to shale play development: A review of successful approaches to wards shale play stimulation in the last two decades. In Proceedings of the Canadian Unconventional Resources and International Petroleum Conference, Calgary, AB, Canada, 19–21 October 2010; pp. 133–874.
23. De, S.; Sengupta, D. Brittleness estimation and mineralogical analysis for evaluation of fracturability: Application to the Cambay Shale, Gujarat, India. In Proceedings of the American Geophysical Union, Fall Meeting 2020, Online, 1–17 December 2020.
24. Fang, X.; Feng, H.; Zhang, Z.; Li, F. Brittleness index prediction method of tight reservoir based on grey correlation and analytic hierarchical process. *Pet. Sci. Technol.* **2023**, 1–25. [CrossRef]
25. Mullen, M.J.; Enderlin, M.B. Fracability Index-More Than Rock Properties. In Proceedings of the SPE Annual Technical Conference and Exhibition, San Antonio, TX, USA, 8–10 October 2012.
26. Junliang, Y.; Jingen, D.; Dingyu, Z.; Dahua, L.; Wei, Y.; Chaogang, C.; Lijun, C.; Zijian, C. Fracability evaluation of shale gas reservoirs. *Acta Pet. Sin.* **2013**, *34*, 523–527. [CrossRef]
27. Li, H. Research progress on evaluation methods and factors influencing shale brittleness: A review. *Energy Rep.* **2022**, *8*, 4344–4358. [CrossRef]
28. Bai, X.; Li, Z.; Lai, F.; Wang, L.; Wu, D. Method for evaluation of engineering sweet spots tight sandstone reservoir production wells. *Arab. J. Geosci.* **2021**, *14*, 2826. [CrossRef]
29. *GB/T50266–99*; The National Standards Compilation Group of People's Republic of China. Standard for Tests Method of Engineering Rock Masses. Planning Press: Beijing, China, 1999.
30. *SL264–2001*; The Professional Standard Compilation Group of People's Republic of China. Specifications for Rock Tests in Water Conservancy and Hydroelectric Engineering. Water Power Press: Beijing, China, 2001.
31. Guo, H.; Aziz, N.I.; Shmidt, L.C. Rock fracture toughness determination by the Brazilian test. *Eng. Geol.* **1993**, *33*, 177–178. [CrossRef]
32. Atkinson, C.; Smelser, R.E.; Sanchez, J. Combined mode fracture via the cracked Brazilian disk test. *Int. J. Fract.* **1982**, *18*, 279–291. [CrossRef]
33. Awaji, H.; Sato, S. Combined mode fracture toughness measurement by the disk test. *J. Eng. Mater. Technol.* **1978**, *100*, 175–182. [CrossRef]
34. Chunlin, L.; Norlund, E. Assessment of damage in rock using the Kaiser effect of acoustic emission. *Int. J. Rock Mech. Min. Sci. Geomech. Abstr.* **1993**, *30*, 943–946.
35. Holcomb, D.J.; Costin, L.S. Detecting damage surfaces in brittle materials using acoustic emissions. *J. Appl. Mech.* **1986**, *208*, 356–544. [CrossRef]
36. Holcomb, D.J. General theory of the Kaiser effect. *Int. J. Rock. Mech. Sci. Geomech. Abstr.* **1993**, *30*, 929–935. [CrossRef]
37. Yongdong, J.; Xuefu, X.; Jiang, X. Research on application of Kaiser effect of acoustic emission to measuring initial stress in rock mass. *Rock Soil Mech.* **2005**, *26*, 946–950.
38. Hu, Y.; Guo, Y.; Qing, H.; Hou, Y. Study on influencing factors and mechanism of pore compressibility of tight sandstone reservoir—A case study of upper carboniferous in ordos basin. *Front. Earth Sci.* **2023**, *10*, 1100951. [CrossRef]

39. Dou, L.; Zuo, X.; Qu, L.; Xiao, Y.; Bi, G.; Wang, R.; Zhang, M. A New Method of Quantitatively Evaluating Fracability of Tight Sandstone Reservoirs Using Geomechanics Characteristics and In Situ Stress Field. *Processes* **2022**, *10*, 1040. [CrossRef]
40. Xu, W.; Zhao, J.; Xu, J. Fracability Evaluation Method for Tight Sandstone Oil Reservoirs. *Nat. Resour. Res.* **2021**, *30*, 4277–4295. [CrossRef]
41. Li, J.; Li, X.R.; Zhan, H.B.; Song, M.S.; Liu, C.; Kong, X.C.; Sun, L.N. Modified method for fracability evaluation of tight sandstones based on interval transit time. *Sci. Lett.* **2020**, *17*, 477–486. [CrossRef]
42. Zhang, D.; Ranjith, P.G.; Perera, M.S.A. The brittleness indices used in rock mechanics and their application in shale hydraulic fracturing: A review. *J. Pet. Sci. Eng.* **2016**, *143*, 158–170. [CrossRef]
43. Obert, L.; Duvall, W.I. *Rock Mechanics and the Design of Structures in Rock*; John Wiley: New York, NY, USA, 1967; pp. 78–82.
44. Ramsay, J.G. *Folding and Fracturing of Rocks*; Mc Graw-Hill: London, UK, 1967; pp. 44–47.
45. Reuss, A. Berechnung der flieβgrenze von mischkristallen aufgrund der plastizitätsbedingung für einkristalle. *ZAMM J. Appl. Math. Mech.* **1929**, *99*, 49–58. [CrossRef]
46. Jarvie, D. Finding bypassed or overlooked pay zones using geo-chemistry techniques. In Proceedings of the International Petroleum Technology Conference, Kuala Lumpur, Malaysia, 3–5 December 2008; pp. 12–18.
47. Rickman, R.; Mullen, M.; Petre, E.; Grieser, B.; Kundert, D. A practical use of shale petrophysics for stimulation design optimization: All shale plays are not clones of the Barnett Shale. In Proceedings of the SPE Annual Technical Conference and Exhibition, Denver, CO, USA, 21–24 September 2008; pp. 115–258.
48. Shuqian, D.; Xiating, F.; Quan, J.; Dingping, X.; Hong, X.; Guofeng, G. Experimental study of mechanical properties of staggered zones under loading and unloading conditions of high stresses. *Chin. J. Rock Mech. Eng.* **2016**, *35*, 1090–1101.
49. Zoback, M.D.; Kohli, A.; Das, I.; McClure, M. The importance of slow slipon faults during hydraulic fracturing stimulation of gas shale reservoirs. In Proceedings of the SPE Americas Unconventional Resources Conference, Pittsburgh, PA, USA, 5–7 June 2012.
50. Jianmeng, S.; Zhilei, H.; Ruibao, Q.; Jinyan, Z. Log evaluation method of fracturing performance in tight gas reservoir. *Acta Pet. Sin.* **2015**, *36*, 74–80.
51. Lavrov, A. The Kaiser effect in rocks: Principles and stress estimation techniques. *Int. J. Rock Mech. Min. Sci.* **2003**, *40*, 151–171. [CrossRef]
52. Saaty, T.L. *The Analytic Hierarchy Process*; McGraw Hill: New York, NY, USA, 1980.
53. Saaty, T.L.; Vargas, L.G.; Dellmann, K. The allocation of intangible resources: The analytic hierarchy process and linear programming. *Socio-Econ. Plan. Sci.* **2003**, *37*, 169–184. [CrossRef]
54. Vaidya, O.S.; Kumar, S. Analytic hierarchy process: An overview of applications. *Eur. J. Oper. Res.* **2006**, *169*, 1–29. [CrossRef]
55. Ying, T.; Yun, X.; Lezhong, L.; Binhai, Z.; Shixin, J. Influence factors and evaluation methods of the gas shale fracability. *Earth Sci. Front.* **2012**, *19*, 356–363.
56. Li, H.; Li, H.; Wang, K.; Liu, C. Effect of rock composition microstructure and pore characteristics on its rock mechanics properties. *Int. J. Min. Sci. Technol.* **2018**, *28*, 303–308. [CrossRef]
57. Price, N.J. *Fault and Joint Development in Brittle and Semi-Brittle Rock*; Pergamon Press: Oxford, UK, 1966; pp. 221–240.
58. Wen-Long, D.; Chao, L.; Chun-Yan, L.I.; Chang-Chun, H.U.; Kai, J.; Wei-Te, C. Dominant factor of fracture development in shale and its relationship to gas accumulation. *Earth Sci. Front.* **2012**, *19*, 212–220.
59. Mian, C.; Yan, J. Study on the experiment for fracture toughness under confining pressure. *Mech. Eng.* **2001**, *23*, 32–35.
60. Yan, J.; Xudong, Z. Determination of fracture toughness for deep well rock with geophysical logging data. *Chin. J. Rock Mech. Eng.* **2001**, *20*, 454–456.
61. Yan, J.; Mian, C.; Huaiying, W.; Yang, Y. Study on prediction method of fracture toughness of rock mode II by logging data. *Chin. J. Rock Mech. Eng.* **2008**, *27*, 3630–3635.
62. Yin, S.; Ding, W.; Zhou, W.; Shan, Y.; Xie, R.; Guo, C.; Wang, R.; Wang, X. In situ stress field evaluation of deep marine tight sandstone oil reservoir: A case study of Silurian strata in northern Tazhong area, Tarim Basin, NW China. *Mar. Pet. Geol.* **2017**, *80*, 49–69. [CrossRef]